Mon. Not. R. Astron. Soc. **000**, 000–000 (0000) Printed 12 January 2013 (MN LaTeX style file v2.2)

arXiv:1102.4269v2 [astro-ph.CO] 15 Jun 2011

Properties of fossil groups in cosmological simulations and galaxy formation models

Weiguang Cui[1,2,5⋆], Volker Springel[3,4,2], Xiaohu Yang[1], Gabriella De Lucia[6], and Stefano Borgani[5,6,7]

[1] *Key Laboratory for Research in Galaxies and Cosmology, Shanghai Astronomical Observatory; the Partner Group of MPA; Nandan Road 80, Shanghai 200030, China*
[2] *Max-Planck-Institut für Astrophysik, Karl-Schwarzschild-Straße 1, 85740 Garching bei München, Germany*
[3] *Heidelberg Institute for Theoretical Studies, Schloss-Wolfsbrunnenweg 35, 69118 Heidelberg, Germany*
[4] *Zentrum für Astronomie der Universität Heidelberg, Astronomisches Recheninstitut, Mönchhofstr. 12-14, 69120 Heidelberg, Germany*
[5] *Astronomy Unit, Department of Physics, University of Trieste, via Tiepolo 11, I-34131 Trieste, Italy*
[6] *INAF, Osservatorio Astronomico di Trieste, via Tiepolo 11, I-34131 Trieste, Italy*
[7] *INFN – National Institute for Nuclear Physics, Trieste, Italy*

12 January 2013

ABSTRACT

It has been a long-standing question whether fossil groups are just sampling the tail of the distribution of ordinary groups, or whether they are a physically distinct class of objects, characterized by an unusual and special formation history. To study this question, we here investigate fossil groups identified in the hydrodynamical simulations of the GIMIC project, which consists of resimulations of five regions in the Millennium Simulation (MS) that are characterized by different large-scale densities, ranging from a deep void to a proto-cluster region. For comparison, we also consider semi-analytic models built on top of the MS, as well as a conditional luminosity function approach. We identify galaxies in the GIMIC simulations as groups of stars and use a spectral synthesis code to derive their optical properties. The X-ray luminosity of the groups is estimated in terms of the thermal bremsstrahlung emission of the gas in the host halos, neglecting metallicity effects. We focus on comparing the properties of fossil groups in the theoretical models and observational results, highlighting the differences between them, and trying to identify possible dependencies on environment for which our approach is particularly well set-up. We find that the optical fossil fraction in all of our theoretical models declines with increasing halo mass, and there is no clear environmental dependence. Combining the optical and X-ray selection criteria for fossil groups, the halo mass dependence of the fossil groups seen in optical vanishes. Over the GIMIC halo mass range we resolve best, $9.0 \times 10^{12} \sim 4.0 \times 10^{13} h^{-1}\,\mathrm{M}_{\odot}$, the central galaxies in the fossil groups show similar properties as those in ordinary groups, in terms of age, metallicity, color, concentration, and mass-to-light ratio. And finally, the satellite galaxy number distribution of fossil groups is consistent with that of non fossil groups. These results support an interpretation of fossil groups as transient phases in the evolution of ordinary galaxy groups rather than forming a physically distinct class of objects.

Key words: clusters: fossil groups – galaxies: formation

1 INTRODUCTION

Galaxy formation is one of the most complex processes in the evolution of the Universe, and many aspects of it are still poorly understood. Based on the hierarchical formation hypothesis, galaxy clusters and groups form through the assembly of many galaxies into a large common dark matter halo. Information about the merging history within a group is carried mainly by its primary central galaxy and the satellite galaxies. If evolved in isolation for a long time, the end-product of the merging in a group should be a system with a central early-type galaxy, and few left-over satellites. Groups

---

[⋆] wgcui@oats.inaf.it

© 0000 RAS

with a strongly dominating central early-type galaxy, and a bright extended X-ray halo with a cooling time scale longer than the group merging timescale, have been called "fossil groups" – because such an outcome could be most easily understood if these are groups with a very early assembly, leaving enough time for $L_\star$ satellite galaxies to merge away with the centre.

After being originally discovered by Ponman et al. (1994), Jones et al. (2003) defined fossil groups (FGs) by requiring that these groups need to have a difference in absolute R-band magnitude of at least $\Delta M_{12} > 2$ mag between the brightest and the second brightest galaxy located within half the projected virial radius, and that their X-ray luminosity should exceed $L_{\mathrm{X,bol}} \gtrsim 2.13 \times 10^{42} h^{-2}$erg s^{-1}. FGs have since been analyzed in numerous observational studies (e.g. Jones et al. 2003; La Barbera et al. 2009; Santos et al. 2007; Mendes de Oliveira et al. 2006; Aguerri et al. 2011). However, due to a rather low number of FGs identified observationally and the lack of X-ray information in many cases, most works focused on the magnitude gap. This magnitude gap has been studied in theoretical work through large sky surveys (e.g. van den Bosch et al. 2007; Yang et al. 2008; Milosavljević et al. 2006), pure dark matter simulations (e.g. D'Onghia et al. 2007; von Benda-Beckmann et al. 2008), semi-analytical models (e.g. Sales et al. 2007; Díaz-Giménez et al. 2008), or through gas simulations (Dariush et al. 2007). However, these studies do not agree well on the optical fossil fraction.

A common theme driving many of these investigations has been the desire to understand whether fossil groups are a class of objects that are special in their formation history (D'Onghia et al. 2005; Dariush et al. 2007; von Benda-Beckmann et al. 2008), and whether they would show different environmental dependences than ordinary groups (von Benda-Beckmann et al. 2008; Díaz-Giménez et al. 2011). Some conflicting claims about this have been made, and it is not yet clear whether fossil groups can be easily accommodated in the leading ΛCDM model for cosmic structure formation.

In this paper, we study the environment of fossil groups in the *Galaxies Intergalactic Medium Interaction Calculation* (GIMIC) simulations, as well as in two semi-analytic models (SAM) of galaxy formation, and one conditional luminosity function (CLF) catalogue. Furthermore, we also investigate the properties of central galaxies in FGs and non-FGs through the GIMIC simulations. The GIMIC runs consist of re-simulations of five different density regions selected from the volume of the Millennium Simulation (MS, Springel et al. 2005). By identifying fossil groups in these regions, we can study in detail how the large-scale environment impacts the properties of these systems, and for the first time, we can carry out such an analysis in full hydrodynamic simulations that start directly from cosmological initial conditions. Furthermore, since the regions of GIMIC are drawn from the MS, we can readily use the SAM catalogues of De Lucia & Blaizot (2007, hereafter D07), and Bower et al. (2006, hereafter B06), to carry out a region-by-region comparison. In addition, the galaxy catalogues based on the conditional luminosity function model of Yang (2011, hereafter CLF) have also been constructed for the MS halos; we can hence select the same five regions here as well. The comparison of these catalogues for the same regions yields insightful tests of the predictions of the theoretical models with respect to FG properties. We also compare the predictions of these models with relevant observational data to assess how closely the models reproduce the observed FG properties.

This paper is organized as follows. In Section 2, we introduce the GIMIC simulations, and describe our methods to analyze the runs in terms of a spectral synthesis code to compute galaxy properties and a simple approach to calculate the X-ray luminosity of host halos. In Section 3, the SAM and CLF catalogues we use are introduced. Section 4 is devoted to a description of the properties of the galaxy populations in the different model catalogues. A comparison of the properties of FGs from these models is presented in Section 5, along with their comparison with observational data. Finally, we discuss our results and summarize our main conclusions in Section 6.

2 ANALYSIS OF THE GIMIC SIMULATIONS

2.1 Simulation set and galaxy identification

In the "Galaxies Intergalactic Medium Interaction Calculation" (GIMIC) project, five different regions of comoving radius $\sim 20\ h^{-1}$ Mpc were selected from the volume of the Millennium Simulation (Springel et al. 2005) and re-simulated with hydrodynamics included. The five regions have different mean over-densities that deviate by $(-2, -1, +0, +1, +2)\,\sigma$ from the cosmic mean, where σ is the rms mass fluctuation on a scale of $\sim 20\ h^{-1}$ Mpc at $z = 1.5$. The simulations included physics modules for gas cooling and photoionization, quiescent star formation associated with supernovae feedback, kinetic supernova feedback and chemodynamics, but no AGN feedback. The GIMIC simulations were run with GADGET-3, an updated version of the GADGET-2 code (last described in Springel 2005), with the physics implementation corresponding to one of the models studied in the 'Overwhelmingly Large Simulations' project (Schaye et al. 2010). The GIMIC regions have been each evolved separately, and were run at several different resolutions. The mass of the gas particles in the GIMIC simulations was $\sim 10^7 h^{-1}\,\mathrm{M}_\odot$, sufficient to make the galaxy catalog complete down to a r-band absolute magnitude limit of about −11.0. Throughout this paper, we adopt the same cosmological parameters as used in GIMIC and the parent MS project: $\Omega_m = 0.25$, $\Omega_\Lambda = 0.75$, $\Omega_b = 0.045$, $n_s = 1$, $\sigma_8 = 0.9$, $H_0 = 100\ h$ km s^{-1} Mpc^{-1} with $h = 0.73$. A detailed description of further methodological aspects of the GIMIC simulations can be found in Crain et al. (2009).

Halos in the simulation were identified by the standard friends-of-friends (FOF) algorithm, applied to the high-resolution dark matter particles with a linking length of $b = 0.2$ in units of the mean inter-particle separation. Baryonic particles were linked to groups by associating them with the group containing the nearest high-resolution dark matter particle. Substructures within FOF halos were then identified with the SUBFIND algorithm (Springel et al. 2001; Dolag et al. 2009), which decomposes each FOF group into a set of locally overdense and gravitationally bound structures. For the larger FOF halos of group- or cluster-size, this procedure reliably identifies the different constituent galaxies that make up the groups. These appear as different subhalos inside the FOF groups, and can be directly compared to observed galaxies.

In optical observations, it has been found recently that not all the emission comes from stars that reside in the cluster's member galaxies. Instead, there is also a smoothly distributed stellar component which is typically peaked around the cluster's central galaxy, but extends to large radii. This diffuse stellar component has been studied in a number of works. For instance, Murante et al. (2007) and Puchwein et al. (2010) analysed high-resolution hydrodynamical simulations of galaxy clusters, and pointed out that this intra-cluster light (ICL) component accounts for up to $\sim$ 45% of all the light in simulated clusters and groups. This means we have to take this ICL component into consideration and can not simply add it to the luminosity of the central group galaxy, which would artificially boosts its luminosity. Puchwein et al. (2010) discussed four different methods to identify the ICL component, all of them showing quite similar results. So we here simply follow their simplest method, limiting the aperture, to exclude the ICL of central galaxies. The cut radius is given by

$$r_{\rm cut} = 27.3\, h^{-1}{\rm kpc} \times \left(\frac{M_{\rm crit200}}{10^{15} h^{-1}\,{\rm M}_\odot}\right)^{0.29}, \qquad (1)$$

where $M_{\rm crit200}$ is the mass within the radius enclosing a mean overdensity 200 times the critical density of the Universe. In Figure 1, we show the measured luminosity function of galaxies in GIMIC, with (red solid line) and excluding (red dotted line) the ICL stars. The two luminosity functions are not significantly different. Unless stated otherwise, we will always use central galaxies without ICL component throughout this paper.

2.2 Optical galaxy properties

We treat each stellar particle in the simulations as a simple stellar population with the initial mass function (IMF) of Chabrier (2003), with a mass range of $0.1 - 100\,{\rm M}_\odot$, taking into account the age and metallicity of the star particle. This IMF matches the one that has also been used when running the GIMIC simulations. The spectrum of the stellar population is produced by interpolating the SSP templates of Bruzual & Charlot (2003).

The spectrum of each simulated galaxy is then simply obtained by adding up all the stellar particles' spectra within the same subhalo:

$$L_{\rm tot}(\lambda) = \sum_{i=1}^{N} m_i\, L_{\rm SPP}(t_i, Z_i, \lambda), \qquad (2)$$

where m_i, t_i, and Z_i are the mass, age, and metallicity of stellar particle i, respectively, N is the total number of stellar particles within the subhalo, and $L_{\rm SPP}$ is the intrinsic SED per unit mass interpolated from the SSP templates. Having obtained the spectra, we then apply the SDSS filters in the AB system to get the galaxies' u, g, r, i, and z-band magnitudes. We do not account for dust extinction in our procedure.

2.3 X-ray luminosity of group halos

Because one of the primary criteria often used to distinguish fossil groups from ordinary groups is the X-ray luminosity, we measure this quantity directly in the hydrodynamic simulations for all of our identified groups. We adopt a simple approach to calculate the X-ray luminosities in the GIMIC simulations, where for simplicity we neglect metal lines and only consider the continuous X-ray emission that is due to thermal bremsstrahlung. Neglecting the contribution from metal lines can provide an underestimate of X-ray luminosities, especially at relatively low X-ray temperatures, $T < 3$ keV. This might undersestimate the bumber of X-ray selected fossil groups in our sample, but does not affect their fossil optical properties. We model the hot gas inside subhalos as only containing a primordial mixture of hydrogen and helium, assuming that it is completely ionized and optically thin.

The bolometric X-ray luminosity L_X of a group halo can be obtained by integrating the thermal bremsstrahlung emissivity over the halo's volume. To calculate this integral, we can cast the volume integral into a discrete sum over the SPH particles. This gives

$$\begin{aligned} L_X = \frac{{\rm d}E}{{\rm d}t} &= \kappa \int_V \frac{0.72 g_B\ T^{\frac{1}{2}}\ \rho^2}{m_p^2} {\rm d}V \\ &= \frac{0.864\,\kappa}{m_p^2} \sum_{i=1}^{N} T_i^{\frac{1}{2}} \rho_i\, m_i, \end{aligned} \qquad (3)$$

where g_B is the bolometric Gaunt factor, which we set to 1.2, m_p the proton mass, $\kappa = (\frac{2\pi kT}{3m_e})^{\frac{1}{2}} \frac{2^5 \pi e^6}{3hm_e c^3}$, with m_e for the electron mass, e for the electron charge, and T for the local plasma temperature. In the above equation, the volume element associated with each of the particles is $\Delta V_i = \rho_i / m_i$, where ρ_i and m_i are the SPH density and particle mass for the i-th particle, respectively.

3 SEMI-ANALYTIC AND CONDITIONAL LUMINOSITY FUNCTION MODELS

3.1 Semi-analytic galaxy catalogues

The Millennium Simulation has been used extensively by the Munich and Durham groups to construct so-called semi-analytic galaxy formation models in which the evolution of galaxies is followed based on dark matter merger histories measured from the simulation. The baryonic physics is described at a coarse level with a simplified set of differential equations, allowing it to be integrated forward in time comparatively quickly. The two semi-analytic galaxy formation codes differ in their detailed assumption about the parameterization of the relevant physics, making it interesting to also compare them with each other, prompting us to consider both models.

Full details of the Munich semi-analytic model can be found in Kauffmann & Haehnelt (2000), Springel et al. (2001), De Lucia et al. (2004), and De Lucia et al. (2006), Croton et al. (2006). We here analyze the model by De Lucia & Blaizot (2007, D07), which is itself a modified version of Croton et al. (2006), and includes a prescription for the growth and activity of central black holes

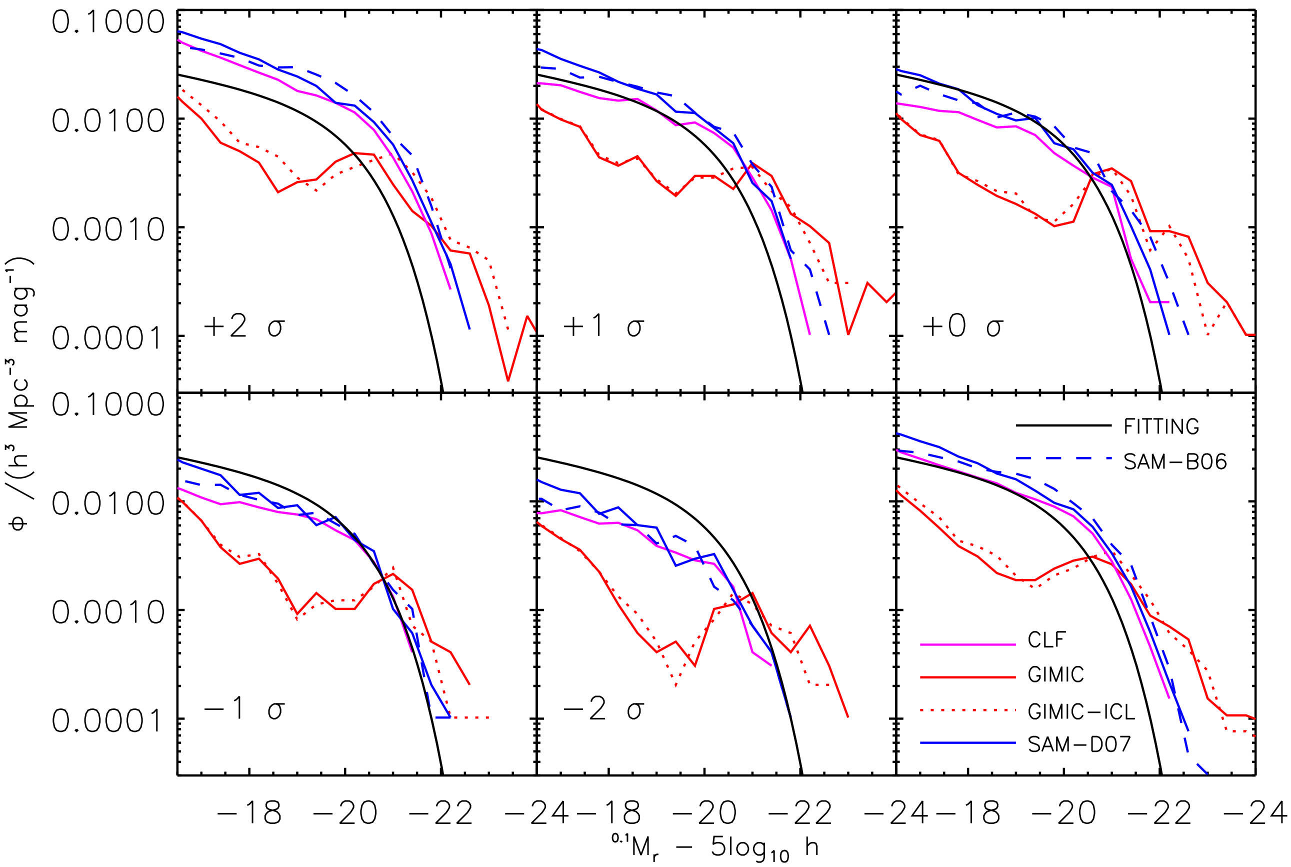

Figure 1. The galaxy luminosity functions of the GIMIC simulations (solid red line), GIMIC simulations without ICL (dotted red lines), the CLF catalogues (solid magenta) of Yang (2011), and the two SAMs from B06 (dashed blue line) and D07 (solid magenta line) in the five different regions we analyzed, labeled as $+2\sigma$ to -2σ from most overdense to most underdense. In all panels, the black solid line shows the Schechter form luminosity fitting function obtained by Blanton et al. (2001) from the SDSS observational data. The lower-right panel shows the averaged luminosity function of the five regions.

and their effect on suppressing the cooling and star formation in massive halos. D07 used the initial mass function of Chabrier (2003). Their publicly available catalogues include 26,787,155 galaxies at $z = 0$ in the whole Millennium volume. The halo mass in this catalogue is $M_{\rm crit200}$, which is defined as mass within the radius enclosing a mean overdensity 200 times the critical density of the Universe. The dust extinction is included in SDSS observer frame magnitudes for this galaxy catalogue.

The Durham semi-analytic galaxy formation model is implemented in the GALFORM code (Cole et al. 2000; Benson et al. 2003; Baugh et al. 2005; Bower et al. 2006). The semi-analytic galaxy catalogue we analyze here is described in detail by Bower et al. (2006, B06), and contains several enhancements compared to older GALFORM models, such as the formation and growth of black holes, disc instabilities, improved cooling calculation and AGN feedback. The B06 model adopts a Kennicutt IMF with no correction for brown dwarf stars. The total number of galaxies number in the final $z = 0$ catalogue is 24,537,589. In this catalogue, dust extinction is also included, but the magnitudes are in the Vega system, which we change to the AB system to match the other catalogues used in this paper.

3.2 Conditional luminosity function catalogues

The conditional luminosity function (CLF) technique is a statistical procedure to populate dark matter halos with galaxies such that the observed galaxy luminosity function (or stellar mass function) and the clustering properties of galaxies can be accurately reproduced. The method has been described in detail by Yang et al. (2003), and has been refined over the years in numerous studies (Yang 2011, and references therein).

In a recent work, Yang (2011) were able to take the full information of subhalo merger histories into account when constructing the CLF as a function of redshift. Here we make use of the model parameters that are constrained using the SDSS luminosity (and stellar mass) function and the projected two point correlation functions. MS dark matter halos are populated with galaxies in two catalogues: one constructed with galaxy luminosities, the other with galaxy stellar masses.

In the luminosity catalogue, each galaxy is assigned an r-band absolute magnitude ${}^{0.1}\mathrm{M}_r - 5\log h$, which is $K + E$ corrected to redshift $z = 0.1$ (Blanton et al. 2003). While in the stellar mass catalogue, the stellar mass is assigned so that we can reproduce the stellar mass function obtained by Yang et al. (2009).

Note that as tested in Yang (2011), the CLF models and thus the constructed galaxy catalogues can not only reproduce the observed SDSS luminosity (stellar mass) functions, but also halo occupation numbers obtained from the SDSS group catalogues. These catalogues contain roughly a total of 10^7 galaxies, slightly less than the two SAM models because of the brighter luminosity (stellar mass) cut.

3.3 Matching of the GIMIC regions and comparing the four models

The spatial location and radius of the five different density regions re-simulated in GIMIC can be found in Table 1 of Crain et al. (2009). It is hence straightforward to cull the semi-analytic models and the CLF catalogues to the same regions. Also, all the models have a parameter that identifies whether a galaxy is the central galaxy in a group, or whether it is a satellite galaxy within a group. We test only the central galaxies for membership in one of the regions, and if this is the case, always use all the galaxies in the same group, too.

The number of galaxies with ${}^{0.1}\mathrm{M}_r - 5\log h \leq -16$ and the number of FOF groups (in brackets) in each region is listed in Table 1. The four models do not agree with each other well in the number of galaxies and the number of FOF groups in all five regions. The reason is that the four models have different predictions for galaxies even in the same dark matter halos. With the magnitude limit we applied, part of low mass galaxies and/or groups are not included. It is interesting to see that the GIMIC model produces fewer galaxies compared to other models in all regions for this magnitude cut, especially in the $+2\sigma$ region. From Figure 1, the drop of Φ in GIMIC is mainly caused by the strong wind model.

Note that since the absolute magnitudes provided in SAMs and GIMIC are scaled to redshift $z = 0$, in order to properly compare with the SDSS observation, we have converted them into the ones corresponding to redshift $z = 0.1$ using the average $K + E$ corrections provided by Blanton et al. (2003); Blanton & Roweis (2007). Throughout the paper we use the same ${}^{0.1}\mathrm{M}_r - 5\log h$ notation. The four models also adopt different definitions of halo masses. For proper comparisons, we convert the halo masses in the SAMs and GIMIC to the ones in the CLF model with a halo abundance matching method. The final halo masses thus correspond to the FOF halos whose mass function is well described by Sheth et al. (2001). We apply this normalized halo mass of each model in the following sections.

4 BASIC SAMPLE PROPERTIES

Before we analyze the specific properties of fossil groups, we study here some of the basic properties of our different model galaxy catalogues, and how they compare to observational data. We limit ourselves to a discussion of the luminosity function, the properties of central galaxies in groups, and the halo occupation distribution function.

4.1 Luminosity function

The luminosity function is one of the most fundamental characteristics of a galaxy population. In Figure 1, we show the GIMIC luminosity function of the five different regions in separate panels, comparing with the observational results of Blanton et al. (2001) and with our semi-analytic and CLF models. A Schechter function fit provides a good description of the dust-corrected SDSS data over a range $-23 < {}^{0.1}\mathrm{M}_r - 5\log h < -16$, with best-fit parameters $\phi_* = 1.46 \times 10^{-2}\, h^3\,\mathrm{Mpc}^{-3}$, $M_\star = -20.83$, and $\alpha = -1.20$. The luminosity functions in the different density regions are clearly different in their normalization. The higher density regions have a higher number density of galaxies, as expected. However, there is no obvious difference in the shape or characteristic magnitude. In the lower-right panel of Figure 1, the total luminosity functions from the CLF and SAM models are also shown; they exhibit a better match than GIMIC to the Schechter fit of Blanton et al. (2001) for the observational data. We note that the CLF and SAM luminosity functions have a higher normalization than the observations. This is mainly due to the fact that we have added all the galaxies in the five regions with equal weight, for simplicity, while in reality there are fewer high density regions than low density regions within a representative volume of the Universe.

It is obvious from Figure 1 that there is a substantial disagreement between the shape of the LF of the GIMIC simulations and the other theoretical models. In fact, the concave shape and bump-like feature in the GIMIC luminosity function appears in all different density regions, and is caused by the specific feedback model that was introduced in the hydrodynamic simulations. In Crain et al. (2009) it was shown that the galaxy stellar mass function has a similar trend (see the right panel of figure 3 in Crain et al. 2009). They also investigated the origin of the disagreement in some detail. At the lower mass end ($M \lesssim 10^9 h^{-1}\,\mathrm{M}_\odot$), the excess number of galaxies reflects a reduction in the efficiency of SNe feedback in poorly resolved galaxies, while at intermediate masses ($10^9 \sim 10^{10} h^{-1}\,\mathrm{M}_\odot$), the ‘dip’ is caused by an efficiency peak in the feedback wind model, that is even too effective in quenching star formation for galaxies in this mass range. Finally, at the high mass end ($M_* \gtrsim 10^{11} h^{-1}\,\mathrm{M}_\odot$), the overprediction of massive galaxies is mainly caused by gas overcooling in the brightest cluster galaxies, which is not efficiently counteracted by SN-driven feedback (see also Saro et al. 2006; Nuza et al. 2010). Resolving this problem may require the introduction of AGN feedback.

Taken at face value, the poorer agreement of the hydrodynamic GIMIC simulations with the observational data may seem to suggest that these calculations are inferior to the other theoretical models. It needs to be taken into account, however, that the hydrodynamic simulations do not involve much tuning, intead they yield a relatively precise and physically self-consistent calculation of the outcome of cosmic evolution for a specific set of assumptions about star formation and its regulation through feedback. The simulations show that it is actually very hard to come up with a successful parameterization of the feedback processes, ar-

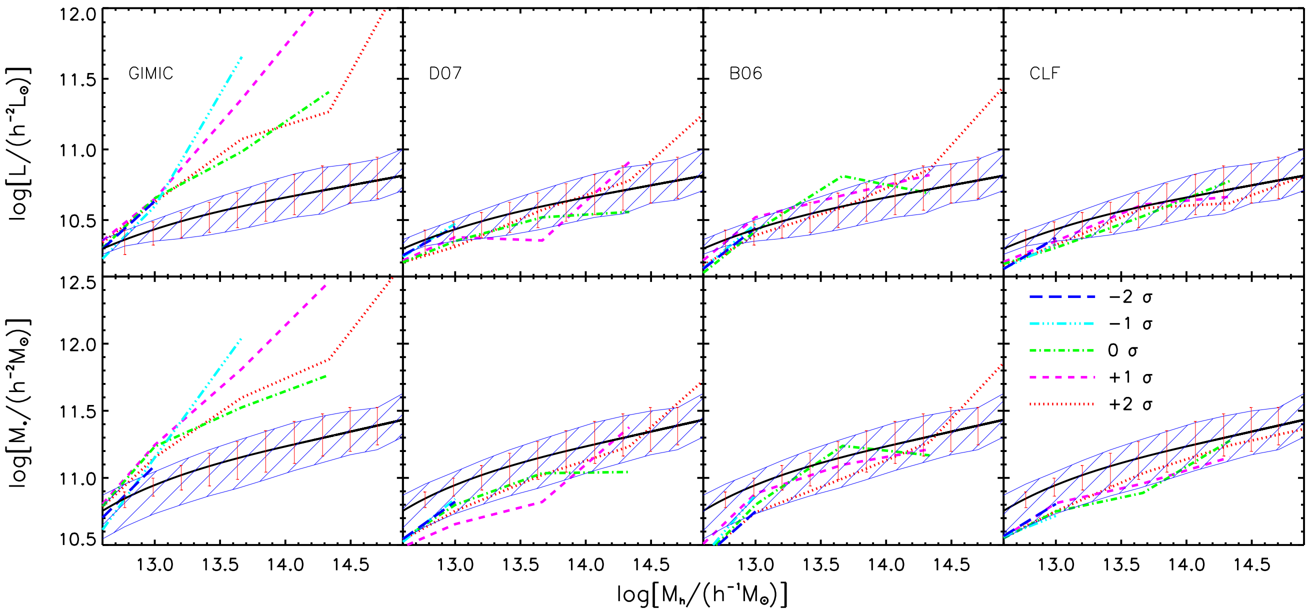

Figure 2. *Upper panels*: Median r-band luminosity of the brightest cluster galaxy (BCG) as function of halo mass of four theoretical models, as labeled. *Lower panels*: Median stellar mass of the most massive galaxy (MMG) as function of halo mass of the models. The solid lines in each panel give the results for the first ranked galaxies in the groups. The different colors and line styles encode the different density regions, according to the key shown in the lower-right panel. For comparison, the solid black line shows the fitting formula of Yang et al. (2008) derived for the CLF model. The shaded area and error bars come from Yang et al. (2008), and show the 68% confidence regions of halo mass estimated through the group luminosity M_L and group stellar mass M_S, respectively.

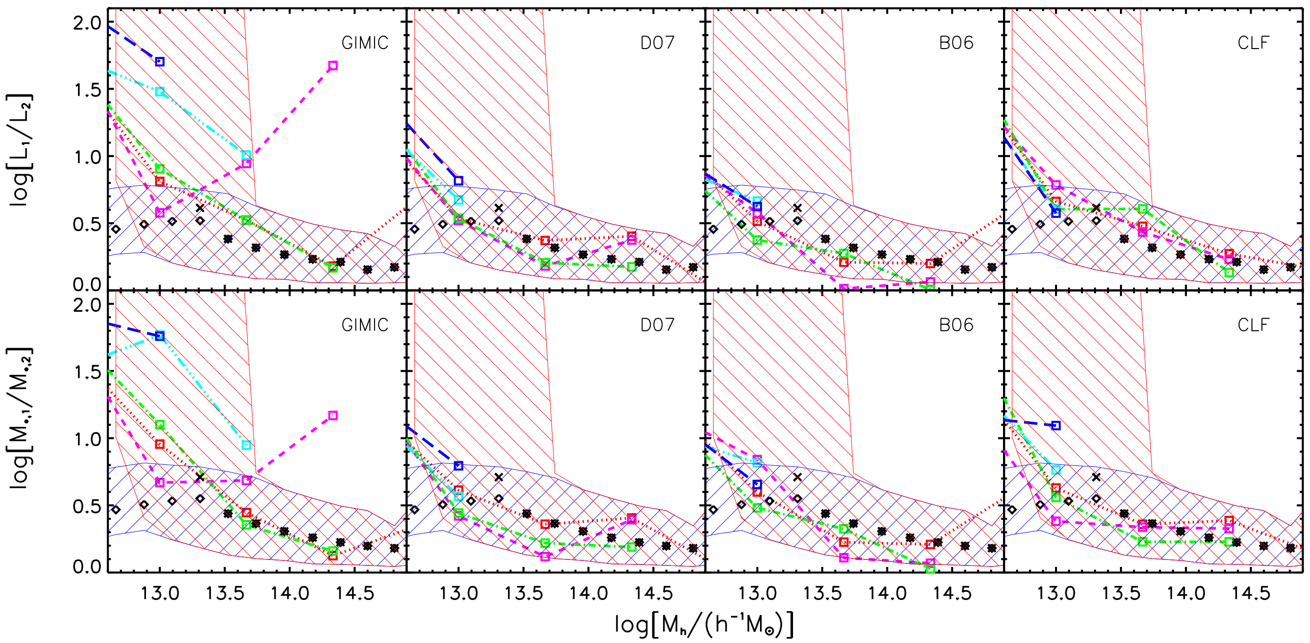

Figure 3. *Upper panels:* The luminosity ratio between first and second ranked galaxies, as a function of halo mass for our four theoretical models, as labeled. *Lower panels:* The stellar mass ratio between first and second ranked galaxies as a function of halo mass for the same models. The colored lines encode the different density regions, using the same key as in Figure 2. The cross and square symbols represent an analysis of the observational data, only differing in the treatment of the second brightest galaxy (Yang et al. 2008). The shaded areas come from Yang et al. (2008), which indicate the corresponding 68% confidence intervals for crosses (red shaded region) and squares (blue shaded region).

Model	$+2\sigma$	$+1\sigma$	0σ	-1σ	-2σ
GIMIC	4,732 (2,583)	1,418 (809)	1,046 (651)	898 (678)	591 (471)
D07	14,516 (7,386)	3,576 (2,226)	2,394 (1,500)	1,957 (1,525)	1,261 (1,022)
B06	10,217 (5,298)	2,431 (1,512)	1,547 (961)	1,212 (958)	736 (620)
CLF	13,553 (5,256)	2,188 (1,610)	1,437 (1,060)	1,303 (1,115)	822 (732)

Table 1. The raw number of galaxies with ${}^{0.1}\mathrm{M}_r - 5\log h < -16$ in the five regions in each of the different theoretical galaxy catalogues. For reference, the second numbers given in brackets list the number of FOF-groups to which the galaxies belong.

guably harder than it may seem based on the success of the semi-analytic models. This clearly indicates that the effect of relevant feedback processes is still poorly understood in direct hydrodynamical simulations. However, one should also remember that the success of SAMs in reproducing luminosity function data is also the result of a tuning of the parameters entering the models.

4.2 The properties of central galaxies

To investigate the suitability of GIMIC, SAM and CLF galaxy populations for fossil groups, we next consider properties of the brightest cluster galaxy (BCG) and the second brightest galaxy. Yang et al. (2008), based on the galaxy groups extracted from SDSS DR4, produced two fitting formulae for the relation between the luminosity of BCGs and the halo mass (Eq. 6 in Yang et al. 2008), as well as for the relation of stellar mass of the most massive galaxy (MMG) and the halo mass (Eq. 7 in Yang et al. 2008). The halo masses in their group catalogues, and thus in the two fitting formulae, are estimated though the ranking of the characteristic group luminosity M_L and the ranking of the characteristic group stellar mass M_S (see more details in Yang et al. 2007). The two sets of halo masses agree reasonably well with each other. Note however that the halo masses in their models are obtained for the WMAP3 cosmology. For consistency, we here converted the halo masses in their models to the ones corresponding to the MS using the abundance matching method. We use these converted fitting formulae as a reference standard. The different halo masses of each model are normalized to the CLF model, as described in Section 3. The selection of the central galaxy data from our simulation is the same as in Yang et al. (2008): either the brightest cluster galaxy (BCG) or the most massive cluster galaxy (MCG) is taken as the central galaxy. For the "isolated galaxies", we apply a cut with the magnitude limit of ${}^{0.1}\mathrm{M}_r - 5\log h < -16$. To change to a common magnitude system, we adopted for all models an r-band magnitude equal to $r = 4.76$ for the Sun in the AB system (Blanton & Roweis 2007).

In the upper panels of Figure 2, we compare model predictions and observational data for the relation between the r-band luminosity of the BCG and the halo mass. In a similar way, in the lower panels we show the relation between stellar mass of the MMG and halo mass. Different panels are for the different model galaxy catalogues. In each panel, results are shown for the regions at different overdensities. The SAM models and the CLF model both follow the observed relations reasonably well, while the GIMIC simulations show substantial disagreements. The tendency of GIMIC to overpredict the mass of the MMG and the luminosity of the BCG begins at halo masses of $\sim 10^{13}h^{-1}\,\mathrm{M}_\odot$. This overprediction occurs because GIMIC forms too many star particles in the central galaxies at late times.

We now explore the gap between the first and second ranked galaxies. In Figure 3, we show the ratio between the brightest (massive) and the second brightest galaxy versus the mass of the host halo, which is directly related to the fossil characteristics of groups. The cross and diamond symbols included for comparison come from the SDSS (Yang et al. 2008), and correspond to two different treatments adopted in case the second galaxy in a group is not observed, because it is fainter than the SDSS magnitude limit of about $r \sim 17.7$. In the first case, the second brightest (massive) galaxy is treated as having zero luminosity (mass), and is shown with crosses. In the second case, the second brightest (massive) galaxy is treated as the magnitude limit of the SDSS survey (diamonds). The two SAM models and the CLF model all show a better fit to the observational data than GIMIC at halo masses greater than $10^{13}h^{-1}\,\mathrm{M}_\odot$. In lower density regions, the ratio in the CLF model and in the two SAMs also does not show large deviations from the higher density regions, unlike GIMIC; but here no tight observational constraints are available. As the observation prefered, the more massive haloes tend to have smaller luminosity gaps. This is supported by our catalogues, and also consistent with the findings of Skibba et al. (2007, 2011).

4.3 Halo occupation distribution

In Figure 4, we plot the satellite numbers versus halo mass, with a specified magnitude limit, ${}^{0.1}\mathrm{M}_r - 5\log h \le -19.0$, for all models. The fitting formula of Yang et al. (2008) that we include for comparison takes a power law form, $\langle N_s \rangle = (M_h/M_{s,0})^\gamma$, where $\langle N_s \rangle$ is the mean number of satellite galaxies, M_h is the halo mass, and the two parameters $M_{s,0}$ and γ have the best fitting values of $10^{12.77}\,M_\odot$ and 1.06, respectively. After accounting for the cosmology transformation from WMAP3 to Millennium for the fitting formula, and a renormalization of the halo mass to CLF using halo abundance matching method for all the models, the satellite numbers of all the models are roughly consistent with the observed power–law fitting relation from observational data, except at the low halo mass end. Quite interestingly, based on the results shown in Figure 4, we do not see any evidence for environmental dependence of the halo occupation distribution in any of the considered models.

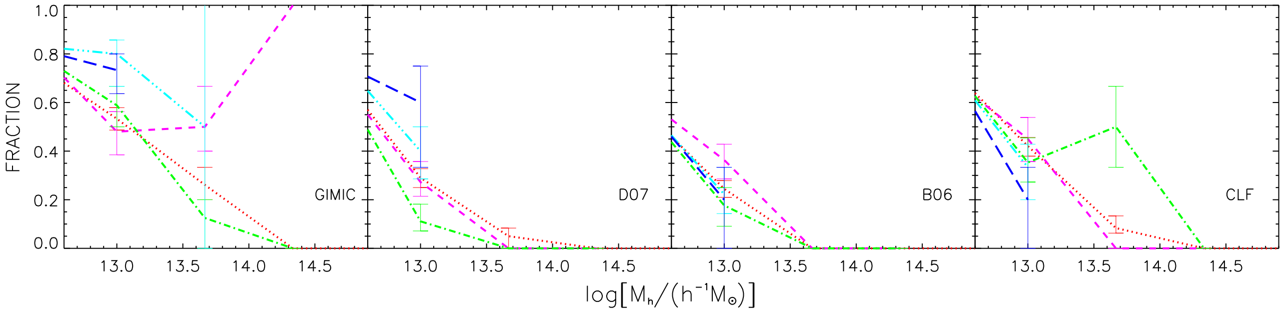

Figure 5. The optical fossil fraction as a function of halo mass for all four theoretical models we analyzed here. Each panel shows the results for one of the catalogues, as labeled. The lines with different colors and styles correspond to the different density regions, as in Fig. 2.

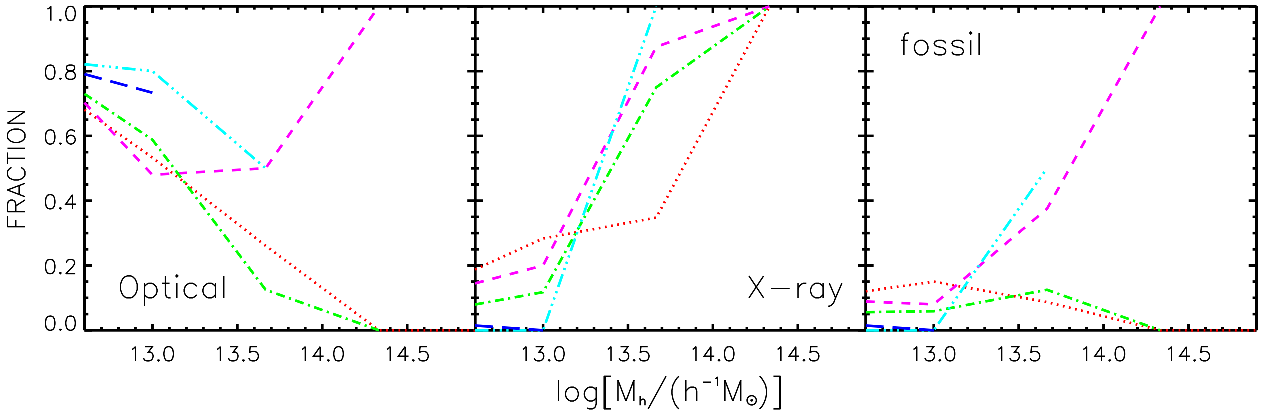

Figure 6. *Left panel:* The optical fossil fraction of GIMIC as a function of halos mass. *Middle panel:* The fraction of GIMIC groups with X-ray luminosity L_X larger than $2.13 \times 10^{42}\ h^{-2}\mathrm{erg\,s^{-1}}$. *Right panel:* The overall fossil fraction when both selection criteria are combined. In each panel, we show results for different overdensities using different colors and styles, based on the same key as in Fig. 2.

5 RESULTS FOR FOSSIL GROUPS

5.1 Abundance of fossil groups in different environments

One of the most important parameters for fossil groups is their abundance. Previous analyses have studied, for example, the 2-degree Field Galaxy Redshift Survey (e.g. van den Bosch et al. 2007), the SDSS-DR4 (Yang et al. 2008), semi-analytic galaxy catalogues (Sales et al. 2007), or cosmological N-body simulations (D'Onghia et al. 2007). Since X-ray data has often been unavailable, many works only considered the magnitude gap between the first and second brightest galaxies, disregarding the requirement for a group to be also X-ray luminous. We note that the predicted optical fossil fractions from these works do not agree particularly well with each other, demonstrating that the uncertainty in this quantity is still high (see Table 2). Interestingly, several studies (D'Onghia et al. 2005; Milosavljević et al. 2006; van den Bosch et al. 2007; Yang et al. 2008; Dariush et al. 2007, 2010) have consistently claimed a trend of an increasing optical fossil fraction with decreasing halo mass.

We start by defining fossil groups based only on the magnitude gap in the r-band, requiring it to be larger than 2 for an optical fossil group, which is the commonly employed definition. In Figure 5, we plot the resulting average optical fossil fraction as a function of halo mass. A mass trend is clearly present in all models. It is not surprising to see such a declining trend in light of what we showed in Figure 3. The strong disagreement in GIMIC (magenta line) is primarily related to the sparseness of the data for the highest halo mass region, and the associated statistical uncertainty. However, the optical fossil fractions in each model are not fully consistent in detail. The error bars in Figure 5 reflect the 1σ scatter obtained from 200 bootstrap resamplings of different groups. All models predict a very high optical fossil fraction at the lower halo mass end. This means that large magnitude gaps become much more common in low mass halos. Taken into account the big error bars, we do not find any clear evidence that environment has an effect on the optical fossil fraction in any of the models.

As we discussed earlier, the hot gas profiles in the GIMIC halos can be used to measure the X-ray luminosity L_X of halos, providing us with a way to arrive at higher specificity in the selection of fossil groups. We now define a group to be fossil only if its X-ray luminosity L_X is larger than $2.13 \times 10^{42}\ h^{-2}\mathrm{erg\,s^{-1}}$, in addition to showing the magnitude gap. This X-ray luminosity limit first adopted by Jones et al. (2003) is meant to exclude normal galaxies which are not elliptical galaxies at the centre of groups,

Mass range ($h^{-1}\,\mathrm{M}_\odot$)	Optical fossil fraction	Fossil fraction	Reference
$10^{13} - 10^{14}$	6.5%	-	van den Bosch et al. (2007)
$10^{12} - 10^{13}$	13.4%	-	van den Bosch et al. (2007)
$\sim 10^{13.5}$	11% – 20%	-	Yang et al. (2008)
$\sim 10^{13}$	18% – 60%	-	Yang et al. (2008)
$1 - 5 \times 10^{13}$	18%	-	D'Onghia et al. (2007)
$\geqslant 10^{13}$	8 – 10	-	Sales et al. (2007)
$\sim 10^{13} - 10^{15}$	13.3%	-	Dariush et al. (2007)
-	-	7.2%	Dariush et al. (2007)
$\sim 10^{13} - 10^{14}$	5 – 40%	-	Milosavljević et al. (2006)
-	-	8 – 20%	Jones et al. (2003)
$\sim 10^{14}$	33%	-	D'Onghia et al. (2005); Sommer-Larsen (2006)

Table 2. Compilation of fossil fractions reported in the literature. In the first column we list the halo mass range for which the estimate applies, and where possible, we distinguish between optical and X-ray based fossil fractions. The last column gives the corresponding references, which here include both theoretical and observational works.

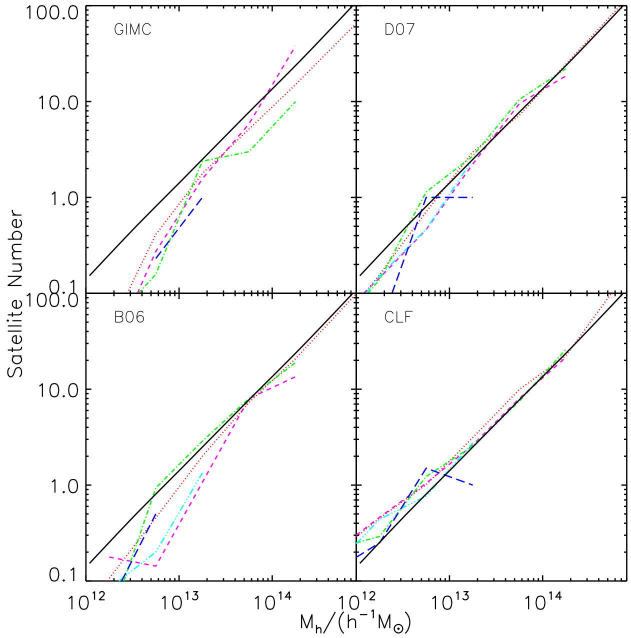

Figure 4. Mean satellite number as a function of halo mass. The colored lines encode the different density regions in the same way as in Fig. 2, for an absolute magnitude limit $^{0.1}\mathrm{M}_r - 5\log h \leq -19.0$. The solid black line is the fitting result by Yang et al. (2008) for the same magnitude limit.

and inevitably imposes a selection bias on the data. In Figure 6, we show the fossil fraction in GIMIC as a function of halo mass based on this definition. In the middle panel of figure 6, we show the fraction of groups that have X-ray luminosity L_X above the threshold $2.13 \times 10^{42}\,h^{-2}\mathrm{erg\,s^{-1}}$. It is not surprising to see that the fractions show an increasing trend with halo mass. Although there are more optical fossil groups in low mass halos, the fossil fraction is very small (less than 15%) due to the limited X-ray luminosity. In general, because of the additional X-ray selection, the halo mass dependence of the fossil groups seen in the optical band vanishes.

Figure 6 also reveals that X-ray bright groups in low density regions are very rare, which appears consistent with the dramatic drop found for low mass halos by Dariush et al. (2007, see their Figure 5). To investigate this reduction of the X-ray fossil fraction in two lower density regions, we further plot the abundance of the groups in L_X-bins for the halo mass range $10^{12} - 10^{15}h^{-1}\,\mathrm{M}_\odot$ in Figure 7. Most of the X-ray luminous groups in the two lower density regions are located around $L_X \sim 10^{38}\,h^{-2}\mathrm{erg\,s^{-1}}$. There are however very rare galaxy groups with $L_X > 2.13 \times 10^{42}\,h^{-2}\mathrm{erg\,s^{-1}}$ in the two lowest density regions. The abundance of systems with $L_X > 2.13 \times 10^{42}\,h^{-2}\mathrm{erg\,s^{-1}}$ within the average density and high density regions are much higher than in the low density regions. The main reason for this behaviour is that structures in low-density regions are generally characterized by shallower potential wells. Therefore, the gas reaches relatively lower densities in the central part of these structures, thus explaining the correspondingly lower X–ray luminosity.

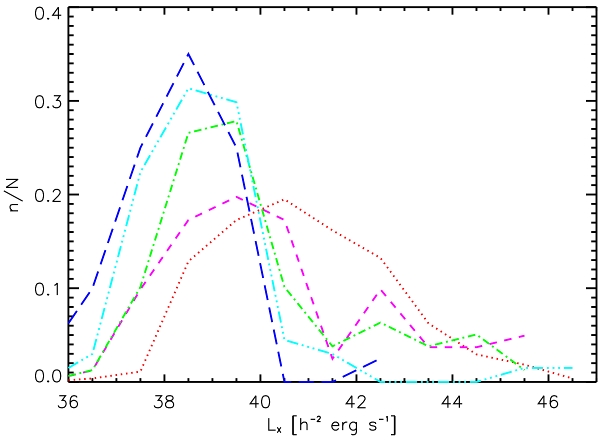

Figure 7. The group abundance as a function of X-ray luminosity. The quantity n shown on the y-axis is the group number in each L_X bin, while N is the total group number. Differently colored and styles lines represent the different density regions, as in Fig. 2.

5.2 The properties of fossil groups

We now focus on the halo mass range $9.0 \times 10^{12} \sim 4.0 \times 10^{13}h^{-1}\,\mathrm{M}_\odot$, which is likely the most reliable in GIMIC. In

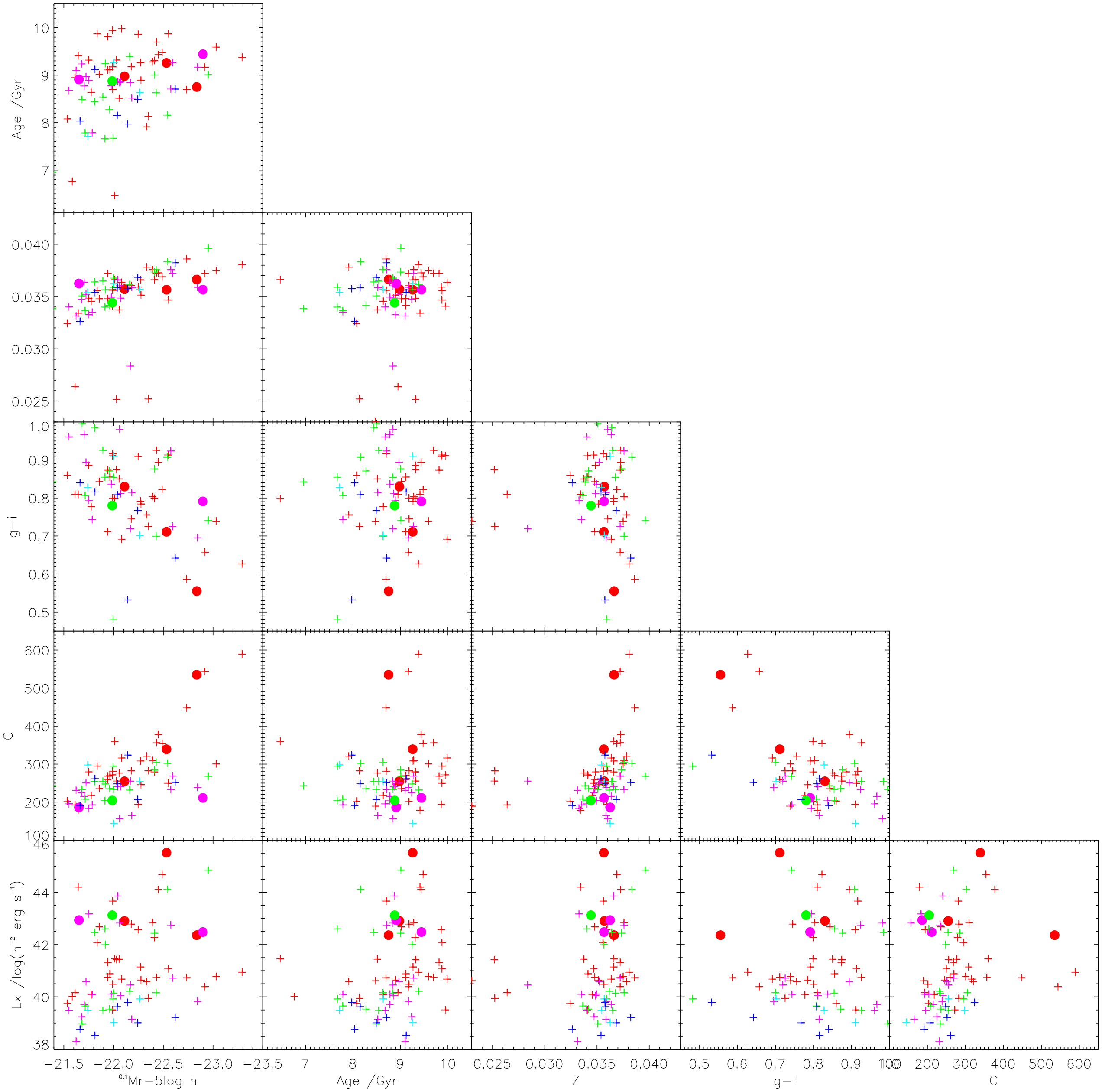

Figure 8. Basic central galaxy properties of fossil and non-fossil groups. The individual panels give the relations between six quantities: the X-ray luminosity L_X, the r band magnitude M_r, the mean age in Gyrs, the mean metallicity Z, the $(g-i)$ color, and the galaxy concentration C. Crosses represent non-fossil groups, while solid circles are for fossil groups. The different colors refer to the different density regions as in our previous figures.

Figure 8, we summarize our measurements for some of the basic properties of the central galaxies of fossil groups and non-fossil groups, such as age, metallicity, colors or concentration, and we discuss them in the following.

Jones et al. (2003) found that fossil groups are more X-ray luminous for a given optical luminosity than non-fossil groups. Using *Chandra* X-ray observations of five fossil groups, supplemented by additional systems from the literature, Khosroshahi et al. (2007) confirmed their result of a L_X-L_R relation. However, a recent work by Voevodkin et al. (2010) reached a different conclusion. They claim that the comparisons in Jones et al. (2003) and Khosroshahi et al. (2007) were affected by systematic errors due to a non-uniform selection, because the data for fossil groups and other systems were obtained separately. Using instead the data from a uniform sample, Voevodkin et al. (2010) concluded that fossil groups are not systematically brighter in X-rays than other groups at the same optical luminosity. Our results in Fig. 8 for the M_r-L_X relation support the conclusion by Voevodkin et al. (2010). In the region

$L_X > 2.13 \times 10^{42}\ h^{-2} \mathrm{erg\,s^{-1}}$, we do not see a systematic increase of the X-ray luminosity for fossil groups at a given optical magnitude.

To quantify the age of our simulated galaxies, we directly use the mean age of the stellar particles. Our results for this analysis are shown in the third row of Figure 8. Fossil groups in these plots typically have a mean age around 9 Gyr, but this age is not significantly enlarged compared to the age of non-fossil groups. This suggests that there may be little justification in the end to call the magnitude-gap selected sample of groups "fossil" – they do not appear to have different ages than normal groups.

Similarly, the mean galaxy metallicities for fossil and non-fossil groups reported in the fourth row of Figure 8 show no apparent differences. We have also used our spectral synthesis code to calculate colors for the simulated galaxies. The $g-i$ color is shown in the fifth row of Figure 8. We here find values that are systematically lower than observational results. That is because we have not introduced any dust attenuation model in our synthesis code, and also because the simulation tends to have too much recent star formation in central galaxies. This is also the reason why the colors of our simulated fossil groups spread over a large range from 0.5 to 1.0 in the plots. Many of them are actually too blue due to recent star formation to represent bona-fide early type galaxies, even though their large stellar mass otherwise suggests that they are.

Finally, the last row in Figure 8 shows the concentration C of the central galaxies. We here used the maximum circular velocity V_{max} of the central galaxy's halo and the radius r_{max} at which this velocity is attained to estimate halo concentrations (Springel et al. 2008). Note that this procedure assumes that the dark matter halo is not substantially modified by the settling of the baryons in the center, and that the rotation curve is dominated by dark matter at its maximum; both of these assumptions may actually break down if the central galaxies are very luminous and compact. Regardless of this complication, we may still go ahead and compare the concentration estimates obtained in this way among the different regions, as done in Fig. 8. We see that although there is one fossil galaxy in the $+2\sigma$ region that shows an unusually high concentration value, most fossil groups are well intermixed with the distribution of normal groups, providing no evidence for a significant difference in the concentrations.

We have also investigated the mass-to-light ratios of the central galaxies in the selected GIMIC data. Previous works (e.g. Khosroshahi et al. 2007; Vikhlinin et al. 1999; Yoshioka et al. 2004) have found conflicting results for the mass-to-light ratio of fossil groups. Using M/L_R Vikhlinin et al. (1999) reported a mass-to-light ratio $\sim 250 - 450 M_\odot/L_\odot$, and using M_{crit200}/L_B Yoshioka et al. (2004) found $\sim 100 - 1000 M_\odot/L_\odot$. Both of these studies claimed a very high mass-to-light ratio for the X-ray overluminous elliptical galaxies, while using M_{vir}/L_B, Khosroshahi et al. (2007) reported that the mass-to-light ratio of fossils tends to be at the upper envelope of the values seen in normal groups and clusters. In Figure 9, we show our measurements for the GIMIC simulation. We use M_{crit200} as the group mass to calculate the mass-to-light ratio. Here we also find that the mass-to-light ratio for fossil groups is consistent with that found for non-fossil groups.

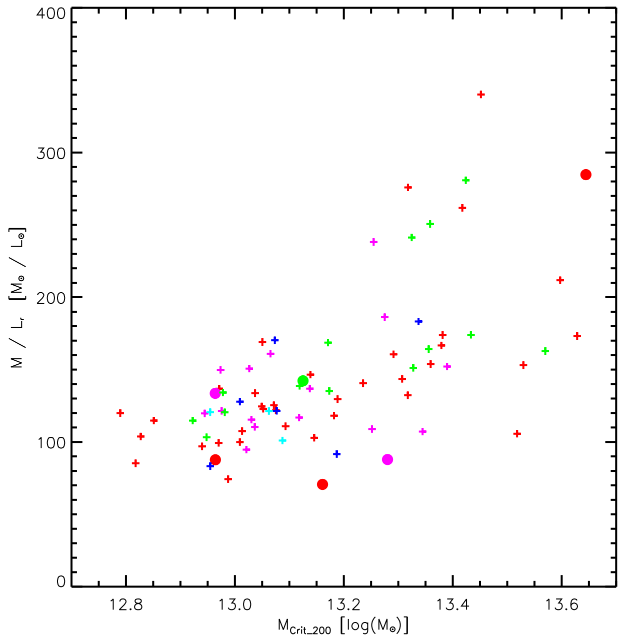

Figure 9. Mass-to-light ratio in the GIMIC simulations as a function of galaxy stellar mass. The crosses are central galaxy's mass-to-light ratio from non-fossil groups, while the solid circles show fossil groups. The different colors encode the different density regions, as in the previous figures.

Based on our results, there is hence little tangible evidence for differences in the properties of fossil and non-fossil groups. In La Barbera et al. (2009), they compared both structural and stellar population properties of fossil and non-fossil group galaxies, which is also shown consistent results. This calls into question whether the fossil groups are indeed a special class of objects that is characterized by an unusual formation history. Instead, our results appear more consistent with an interpretation of fossil groups as a common phase in galaxy evolution during which they lie in the tail of the distribution of a certain group properties, in this case the magnitude difference between first and second ranked galaxies. This result is in line with findings obtained by Dariush et al. (2010), who also used data from the Millennium simulation. These authors found that, no matter at what redshift the fossil groups are selected, after $\sim$ 4Gyr more than $\sim$ 90 percent of them change their status and become non-fossil according to the magnitude gap criterion. This behavior, obtained from the galaxy formation histories, directly supports our conclusion here. As a further check, we show in Figure 10 the number of satellites for fossil and non fossil groups. Here we use all the satellite galaxies in the GIMIC simulations. The satellite number for fossil groups is not different from that obtained considering non fossil groups, which confirms that the fossil groups do not have unusual formation histories. Nevertheless, we stress that although the fossil groups defined according to the magnitude gap are statistically similar to non fossil groups, there may be rare situations in which the fossil groups indeed have unusual formation histories (the few outliers visible in Figure 10).

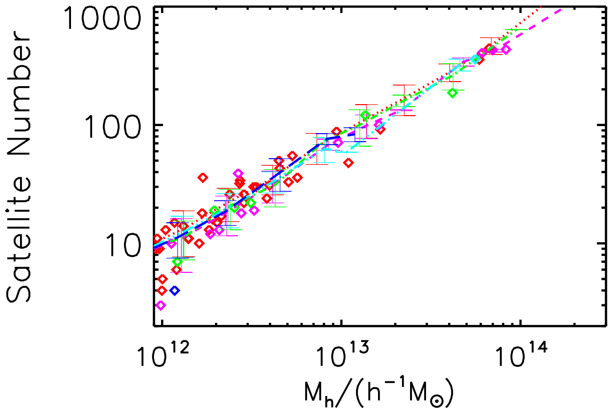

Figure 10. The number distribution of all satellite galaxies in the GIMIC simulations. The different lines are the mean satellite number for non fossil groups, while the diamonds show results for fossil groups. The different colors correspond to different density regions, as in the previous figures. The error bars indicate the r.m.s. scatter within each mass bin.

6 DISCUSSION AND CONCLUSIONS

In this study, we have analyzed fossil groups in the hydrodynamic simulation data of GIMIC combined with CLF catalogues and two semi-analytic galaxy formation models. Our primary goal has been to shed light on the question of how well models of galaxy formation reproduce the observational properties of fossil groups, and whether there is any evidence that this class of objects is characterized by a special formation history. To this end we have first investigated the luminosity functions of our theoretical models, and in particular the abundance of brightest and most massive cluster galaxies. We then considered the ratio of luminosity or stellar mass between the first and second ranked cluster galaxies, and examined the satellite abundance as a function of host halo mass. In all of our measurements, we have also checked whether there is any environmental difference between the five regions simulated by GIMIC, which have substantially different mean densities.

For defining "fossil groups", we have mostly employed the luminosity gap between the two first ranked galaxies in a group, similar to what has been done in many previous works. However, by also measuring the X-ray luminosity of halos in GIMIC, we could more sharply define fossil groups as those which also have high X-ray luminosity, reflecting more closely the originally used observational definition. Since X-ray emission is unavailable in the CLF and the SAMs, we have however applied this selection only in parts of our analysis. Finally, we have investigated some basic properties of fossil and non-fossil groups in order to see in which properties they differ most significantly. For this, we restricted our halo sample to the mass range $9.0 \times 10^{12} \sim 4.0 \times 10^{13} h^{-1}$ M$_\odot$, which should be the most reliable in our hydrodynamical simulations.
Our primary conclusions can be summarized as follows.

- The optical fossil fraction in all of our theoretical models declines with increasing halo mass. However, the models do not agree in detail at a specific halo mass. And we did not find clear evidence that the optical fossil fraction has environmental effects in all the theoretical galaxy formation models.
- After applying the bright X-ray luminosity limit in the selection of fossil groups, the total fraction of fossil groups decreases significantly in small halos. As a consequence, the halo mass dependence of the fossil groups seen in optical vanishes.
- From the L_X distribution of groups identified in the GIMIC simulations, as shown in Figure 7, we have found evidence for a clear environmental effect: halos found in lower-density regions have relatively lower X-ray luminosity. Their median X-ray luminosity can vary by two orders of magnifude, from $\sim 10^{38.5}\ h^{-2}\mathrm{erg\,s^{-1}}$ (-2σ overdensity region in GIMIC) to $\sim 10^{40.5}\ h^{-2}\mathrm{erg\,s^{-1}}$ (2σ overdensity region in GIMIC).
- When we investigated the properties of central galaxies in fossil and non-fossil groups, we have found no differences in the magnitude, X-ray luminosity, age, metallicity, concentration, color or mass-to-light ratio. In particular, the mean ages of the central galaxies in fossil groups are not really 'fossil' in the sense of the word. This casts doubts about whether fossil groups are a useful concept to identify a particular class of early type galaxies.
- In addition, we have checked that the satellite galaxies number distribution of fossil and non-fossil groups. There is not significantly different difference between these two populations as well.

Our results are consistent with the findings of von Benda-Beckmann et al. (2008), who studied a concordance ΛCDM cosmological simulation and pointed out that many groups will go through an 'optical fossil phase' that is typically ended by renewed infall from the environment. In this picture, fossil groups are simply groups that temporarily are in a 'fossil phase', such that a significant difference in the central galaxy properties can not be expected. It is consistent with the analysis carried out by Dariush et al. (2010), using also Millennium data, who found that about 90% fossil groups will become non-fossils after ∼ 4Gyr. The other important result of our analysis is the absence of strong environmental effects at the group scale, at least at the level that could be probed with the limited sample sizes that we had available in the GIMIC regions. It is well possible that there are still weak trends with large-scale overdensity, but uncovering those reliably will require larger simulation volumes.

ACKNOWLEDGEMENTS

The authors would like to thank Lei Liu for the help and discussion of SAM data, Stéphane Charlot for the help of SSP templates of Bruzual & Charlot (2003), and the anonymous referee for constructive comments that greatly improved the presentation of this paper. We also thank Youcai Zhang, Jing Wang, Shiyin Shen, Till Sawala, Klaus Dolag, Pierluigi Monaco for valuable discussions. The semi-analytic galaxy catalogue is publicly available at http://www.g-vo.org/MyMillennium3/

Weiguang Cui acknowledges a fellowship from the European Commission's Framework Programme 7, through the

Marie Curie Initial Training Network CosmoComp (PITN-GA-2009-238356). GDL acknowledges financial support from the European Research Council under the European Community's Seventh Framework Programme (FP7/2007-2013)/ERC grant agreement n. 202781. This work is partly supported by 973 Program (No. 2007CB815402), the CAS Knowledge Innovation Program (Grant No. KJCX2-YW-T05), grants from NSFC (Nos. 10821302, 10925314), by a PRIN09-INAF grant and by the INFN-PD51 grant.

REFERENCES

Aguerri J. A. L., Girardi M., Boschin W., Barrena R., Méndez-Abreu J., Sánchez-Janssen R., Borgani S., Castro-Rodriguez N., et al. 2011, A&A, 527, A143+

Baugh C. M., Lacey C. G., Frenk C. S., Granato G. L., Silva L., Bressan A., Benson A. J., Cole S., 2005, MNRAS, 356, 1191

Benson A. J., Bower R. G., Frenk C. S., Lacey C. G., Baugh C. M., Cole S., 2003, ApJ, 599, 38

Blanton M. R., Dalcanton J., Eisenstein D., et al. et al. 2001, AJ, 121, 2358

Blanton M. R., Hogg D. W., et al. 2003, ApJ, 592, 819

Blanton M. R., Roweis S., 2007, AJ, 133, 734

Bower R. G., Benson A. J., Malbon R., Helly J. C., Frenk C. S., Baugh C. M., Cole S., Lacey C. G., 2006, MNRAS, 370, 645

Bruzual G., Charlot S., 2003, MNRAS, 344, 1000

Chabrier G., 2003, PASP, 115, 763

Cole S., Lacey C. G., Baugh C. M., Frenk C. S., 2000, MNRAS, 319, 168

Crain R. A., Theuns T., Dalla Vecchia C., Eke V. R., Frenk C. S., Jenkins A., Kay S. T., Peacock J. A., Pearce F. R., Schaye J., Springel V., Thomas P. A., White S. D. M., Wiersma R. P. C., 2009, MNRAS, 399, 1773

Croton D. J., Springel V., White S. D. M., De Lucia G., Frenk C. S., Gao L., Jenkins A., Kauffmann G., Navarro J. F., Yoshida N., 2006, MNRAS, 365, 11

Dariush A., Khosroshahi H. G., Ponman T. J., Pearce F., Raychaudhury S., Hartley W., 2007, MNRAS, 382, 433

Dariush A. A., Raychaudhury S., Ponman T. J., Khosroshahi H. G., Benson A. J., Bower R. G., Pearce F., 2010, MNRAS, 405, 1873

De Lucia G., Blaizot J., 2007, MNRAS, 375, 2

De Lucia G., Kauffmann G., White S. D. M., 2004, MNRAS, 349, 1101

De Lucia G., Springel V., White S. D. M., Croton D., Kauffmann G., 2006, MNRAS, 366, 499

Díaz-Giménez E., Muriel H., Mendes de Oliveira C., 2008, A&A, 490, 965

Díaz-Giménez E., Zandivarez A., Proctor R., Mendes de Oliveira C., Abramo L. R., 2011, A&A, 527, A129+

Dolag K., Borgani S., Murante G., Springel V., 2009, MNRAS, 399, 497

D'Onghia E., Maccio' A. V., Lake G., Stadel J., Moore B., 2007, ArXiv e-prints, 0704.2604

D'Onghia E., Sommer-Larsen J., Romeo A. D., Burkert A., Pedersen K., Portinari L., Rasmussen J., 2005, ApJL, 630, L109

Jones L. R., Ponman T. J., Horton A., Babul A., Ebeling H., Burke D. J., 2003, MNRAS, 343, 627

Kauffmann G., Haehnelt M., 2000, MNRAS, 311, 576

Khosroshahi H. G., Ponman T. J., Jones L. R., 2007, MNRAS, 377, 595

La Barbera F., de Carvalho R. R., de la Rosa I. G., Sorrentino G., Gal R. R., Kohl-Moreira J. L., 2009, AJ, 137, 3942

Mendes de Oliveira C. L., Cypriano E. S., Sodré J. L., 2006, AJ, 131, 158

Milosavljević M., Miller C. J., Furlanetto S. R., Cooray A., 2006, ApJL, 637, L9

Murante G., Giovalli M., Gerhard O., Arnaboldi M., Borgani S., Dolag K., 2007, MNRAS, 377, 2

Nuza S. E., Dolag K., Saro A., 2010, MNRAS, 407, 1376

Ponman T. J., Allan D. J., Jones L. R., Merrifield M., McHardy I. M., Lehto H. J., Luppino G. A., 1994, Nature, 369, 462

Puchwein E., Springel V., Sijacki D., Dolag K., 2010, MNRAS, 406, 936

Sales L. V., Navarro J. F., Lambas D. G., White S. D. M., Croton D. J., 2007, MNRAS, 382, 1901

Santos W. A., Mendes de Oliveira C., Sodré J. L., 2007, AJ, 134, 1551

Saro A., Borgani S., Tornatore L., Dolag K., Murante G., Biviano A., Calura F., Charlot S., 2006, MNRAS, 373, 397

Schaye J., Dalla Vecchia C., Booth C. M., Wiersma R. P. C., Theuns T., Haas M. R., Bertone S., Duffy A. R., McCarthy I. G., van de Voort F., 2010, MNRAS, 402, 1536

Sheth R. K., Mo H. J., Tormen G., 2001, MNRAS, 323, 1

Skibba R. A., Sheth R. K., Martino M. C., 2007, MNRAS, 382, 1940

Skibba R. A., van den Bosch F. C., Yang X., More S., Mo H., Fontanot F., 2011, MNRAS, 410, 417

Sommer-Larsen J., 2006, MNRAS, 369, 958

Springel V., 2005, MNRAS, 364, 1105

Springel V., Wang J., Vogelsberger M., Ludlow A., Jenkins A., Helmi A., Navarro J. F., Frenk C. S., White S. D. M., 2008, MNRAS, 391, 1685

Springel V., White S. D. M., Jenkins A., Frenk C. S., Yoshida N., Gao L., Navarro J., Thacker R., Croton D., Helly J., Peacock J. A., Cole S., Thomas P., Couchman H., Evrard A., Colberg J., Pearce F., 2005, Nature, 435, 629

Springel V., White S. D. M., Tormen G., Kauffmann G., 2001, MNRAS, 328, 726

van den Bosch F. C., Yang X., Mo H. J., Weinmann S. M., Macciò A. V., More S., Cacciato M., Skibba R., Kang X., 2007, MNRAS, 376, 841

Vikhlinin A., McNamara B. R., Hornstrup A., Quintana H., Forman W., Jones C., Way M., 1999, ApJL, 520, L1

Voevodkin A., Borozdin K., Heitmann K., Habib S., Vikhlinin A., Mescheryakov A., Hornstrup A., Burenin R., 2010, ApJ, 708, 1376

von Benda-Beckmann A. M., D'Onghia E., Gottlöber S., Hoeft M., Khalatyan A., Klypin A., Müller V., 2008, MNRAS, 386, 2345

Yang X., 2011, In preparation

Yang X., Mo H. J., van den Bosch F. C., 2003, MNRAS, 339, 1057

Yang X., Mo H. J., van den Bosch F. C., 2008, ApJ, 676, 248

Yang X., Mo H. J., van den Bosch F. C., 2009, ApJ, 695, 900

Yang X., Mo H. J., van den Bosch F. C., Pasquali A., Li C., Barden M., 2007, ApJ, 671, 153

Yoshioka T., Furuzawa A., Takahashi S., Tawara Y., Sato S., Yamashita K., Kumai Y., 2004, Advances in Space Research, 34, 2525